

# Synthesis of Wide-Angle Scanning Arrays through Array Power Control

P. Rosatti,<sup>(1)(2)</sup> G. Oliveri,<sup>(1)(2)</sup> *Fellow, IEEE*, and A. Massa,<sup>(1)(2)(3)(4)(5)</sup> *Fellow, IEEE*

<sup>(1)</sup> *ELEDIA Research Center (ELEDIA@UniTN - University of Trento)*

DICAM - Department of Civil, Environmental, and Mechanical Engineering

Via Mesiano 77, 38123 Trento - Italy

E-mail: {*pietro.rosatti, giacomo.oliveri, andrea.massa*}@unitn.it

Website: [www.eledia.org/eledia-unitn](http://www.eledia.org/eledia-unitn)

<sup>(2)</sup> *CNIT - "University of Trento" ELEDIA Research Unit*

Via Sommarive 9, 38123 Trento - Italy

Website: [www.eledia.org/eledia-unitn](http://www.eledia.org/eledia-unitn)

<sup>(3)</sup> *ELEDIA Research Center (ELEDIA@UESTC - UESTC)*

School of Electronic Science and Engineering, Chengdu 611731 - China

E-mail: [andrea.massa@uestc.edu.cn](mailto:andrea.massa@uestc.edu.cn)

Website: [www.eledia.org/eledia-uestc](http://www.eledia.org/eledia-uestc)

<sup>(4)</sup> *ELEDIA Research Center (ELEDIA@TSINGHUA - Tsinghua University)*

30 Shuangqing Rd, 100084 Haidian, Beijing - China

E-mail: [andrea.massa@tsinghua.edu.cn](mailto:andrea.massa@tsinghua.edu.cn)

Website: [www.eledia.org/eledia-tsinghua](http://www.eledia.org/eledia-tsinghua)

<sup>(5)</sup> *School of Electrical Engineering*

Tel Aviv University, Tel Aviv 69978 - Israel

E-mail: [andrea.massa@eng.tau.ac.il](mailto:andrea.massa@eng.tau.ac.il)

Website: <https://engineering.tau.ac.il/>

*This work has been submitted to the IEEE for possible publication. Copyright may be transferred without notice, after which this version may no longer be accessible.*

# **Synthesis of Wide-Angle Scanning Arrays through Array Power Control**

P. Rosatti, G. Oliveri, and A. Massa

## **Abstract**

A new methodology for the synthesis of wide-angle scanning arrays is proposed. It is based on the formulation of the array design problem as a multi-objective one where, for each scan angle, both the radiated power density in the scan direction and the total reflected power are accounted for. A set of numerical results from full-wave simulated examples - dealing with different radiators, arrangements, frequencies, and number of elements - is reported to show the features of the proposed approach as well as to assess its potentialities.

**Key words:** Wide-Angle Scanning; Excitation Design; Array Synthesis; Active Reflection Co-efficient Stabilization; Multi-Objective Evolutionary Optimization.

# 1 Introduction and Rationale

Wide-angle scanning is one of the key requirements in modern antenna arrays for communications and sensing [1][2]. Indeed, stable radiation performance over a wide range of steering angles are increasingly important in several applicative scenarios such as wireless coverage, automotive radars, satellite communications, and imagers [1]-[3]. Unfortunately, the gain/directivity of antenna arrays typically worsens as the scan angle increases, specifically in the presence of “blind spots” [1][2], and it limits the array field-of-view (*FoV*) [1][2]. These undesired phenomena are a direct consequence of the instability of the active return loss (*ARL*) versus the scan angle [4].

In the last decades, several approaches have been introduced in the state-of-the-art (*SoA*) literature to improve the *ARL* stability and to increase the *FoV* of phased arrays by mitigating the inter-element coupling [3][5]-[13]. More in detail, the exploitation of ad-hoc solutions such as the use of cavities [5][6] or magnetic dipoles [7] has been proposed to individually insulate the array elements. An alternative strategy, not involving complex radiators, resorts to the introduction of decoupling feed networks [8][9][14], which synthesis and implementation become very challenging when a wideband working is required [8][9][14]. Wide-angle impedance matching (*WAIM*) layers coating the array and based either on standard [15] or artificial materials [3][10]-[13] has been also adopted to stabilize the *ARL*. Nonetheless, this latter solution - as well as the previous ones - needs non-trivial updates of the system hardware, as applied to existing architectures, and customized designs/implementations strongly depend on the adopted antenna technology [3][10]-[13].

Otherwise, the *ARL* stabilization may be yielded without architectural modifications by considering a completely different perspective, as well. Towards this end, let us notice that the *ARL* depends not only on the inter-element coupling, but also on the excitations applied to each elementary radiator of the array [4][16]. While the synthesis of such excitations is typically aimed at controlling the scan direction, the sidelobe profile [17], and/or more advanced quality-of-service indicators [18][19], there are not theoretical obstacles to even address the stabilization the *ARL* still fulfilling the user-desired pattern features when scanning.

Following this line of reasoning, an innovative methodology for the synthesis of wide-scanning

arrays is proposed into the following. Such an approach is based on the formulation of the array synthesis as a multi-objective problem where, for each scan angle, both the radiated power density in the scan direction and the total reflected power are accounted for by including the finite array coupling in the design process (i.e., no periodicity approximation is employed).

Accordingly, the main innovative contributions of this work include (i) for the first time to the best of the authors' knowledge, the synthesis of the array excitations to minimize the reflected power, while keeping suitable radiation performance, for widening the  $FoV$  in finite arrays, (ii) the full-wave numerical proof for both linear and planar arrays that it is possible to obtain wider scan angles without modifying the antenna architecture, hence implicitly the assessment of the applicability of the proposed concept to upgrade existing arrays, and (iii) the derivation of a general-purpose strategy for wide angle scanning that, unlike  $SoA$  methods [3][5]-[13], can be adopted regardless of the underlying antenna technology and/or physical implementation details.

The outline of the paper is as follows. The mathematical formulation of the array synthesis problem at hand is formulated in Sect. 2, where the proposed excitation-based approach to yield wide-angle scanning performance is presented, as well. A set of numerical results from full-wave simulated examples is reported to show the features of the proposed strategy as well as to assess its potentialities in different working conditions and also in comparison with state-of-the-art competitive techniques (Sect. 3). Finally, some conclusions are drawn (Sect. 4).

## 2 Mathematical Formulation

Let us consider the scenario in Fig. 1 where an antenna array of  $N$  elements, each one described by the  $L$  geometrical parameters  $\underline{g} = \{g_l; l = 1, \dots, L\}$  and operating at the carrier frequency  $f_0$ , is fed by the set of  $N$  incident excitation coefficients  $\underline{w}_q^+ \triangleq \{w_{nq}^+; n = 1, \dots, N\}$  to radiate a beampattern steered at the  $q$ -th ( $q = 1, \dots, Q$ ) scan angle  $(\theta_q, \varphi_q)$  [4][16][20]. The corresponding reflected excitation coefficients, measured at the  $n$ -th ( $n = 1, \dots, N$ ) element, of the array are defined as [16]

$$w_{nq}^- \triangleq w_{nq}^+ \times \Gamma_{nq} \quad (1)$$

where

$$\Gamma_{nq} \triangleq \sum_{m=1}^N S_{nm} \frac{w_{mq}^+}{w_{nq}^+} \quad (2)$$

it the  $n$ -th ( $n = 1, \dots, N$ ) element active reflection coefficient at the  $q$ -th ( $q = 1, \dots, Q$ ) scan angle, the corresponding *ARL* being  $ARL_{nq} \triangleq |\Gamma_{nq}|^2$  ( $n = 1, \dots, N$ ;  $q = 1, \dots, Q$ ) [3][4][10]-[13], and  $S_{nm}$  is the  $(n, m)$ -th ( $n, m = 1, \dots, N$ ) entry of the  $N \times N$  scattering matrix  $\mathcal{S}$  [4][16][17][20]. This latter univocally models the array inter-element coupling effects that, unlike  $\Gamma_{nq}$  (2) and  $w_{nq}^-$  (1), does not depend on the applied array excitations  $w_{nq}^+$ .

Under the above assumptions, the total excitation at the  $n$ -th ( $n = 1, \dots, N$ ) array element,  $w_{nq}$  ( $w_{nq} \triangleq w_{nq}^+ + w_{nq}^-$ ) turns out to be [16][20]

$$w_{nq} = (1 + \Gamma_{nq}) w_{nq}^+, \quad (3)$$

then field radiated by the  $N$ -elements antenna array in the Fraunhofer region has the following expression [16][17][20]

$$\mathbf{E}(\mathbf{r} | \underline{w}_q) = \frac{jk_0 \exp(-jk_0 r)}{2\pi r} \sum_{n=1}^N w_{nq} \exp[-jk_0 (\mathbf{r}_n \cdot \hat{\mathbf{r}})] \mathbf{E}_n(\theta, \varphi), \quad (4)$$

which holds true regardless of the array geometry (linear/planar) and element polarization (i.e., single/dual polarization). In (4),  $k_0$  is the free-space wavenumber,  $\mathbf{r} = \{r, \theta, \varphi\}$  is the spatial coordinate ( $\hat{\mathbf{r}} = \frac{\mathbf{r}}{r}$ ),  $\cdot$  stands for the scalar product, and  $\mathbf{r}_n$  is the location of the  $n$ -th ( $n = 1, \dots, N$ ) array element, which element pattern is  $\mathbf{E}_n(\theta, \varphi)$  [17]. It is worth pointing out that in finite arrays, the element pattern is different for each  $n$ -th ( $n = 1, \dots, N$ ) element [i.e.,  $\mathbf{E}_n(\theta, \varphi) \neq \mathbf{E}_m(\theta, \varphi)$ ,  $n \neq m$  ( $n, m = 1, \dots, N$ )], even though the centrally-located radiators of large arrays exhibit very similar angular responses [17].

The power density radiated along the direction  $(\theta, \varphi)$  by the array steered towards  $(\theta_q, \varphi_q)$  is obtained from (4) as follows

$$\psi_q(\theta, \varphi) = \lim_{r \rightarrow \infty} \frac{r^2}{2\nu} |\mathbf{E}(\mathbf{r} | \underline{w}_q)|^2 \quad (5)$$

and the total radiated power is  $\mathbb{P}_q^{RAD} = \int_{\Omega} \psi_q(\theta, \varphi) d\Omega$ ,  $\Omega$  being a far-field closed surface

surrounding the array. Moreover, the total reflected power percentage is defined as

$$\zeta_q = \frac{\mathbb{P}_q^{REFL}}{\mathbb{P}_q^{IN}} \quad (6)$$

where  $\mathbb{P}_q^{IN}$  and  $\mathbb{P}_q^{REFL}$  are the input power ( $\mathbb{P}_q^{IN} \triangleq \sum_{n=1}^N |w_{nq}^+|^2$ ) and the reflected power ( $\mathbb{P}_q^{REFL} \triangleq \sum_{n=1}^N |w_{nq}^-|^2$ ) equal to  $\mathbb{P}_q^{REFL} \triangleq \sum_{n=1}^N ARL_{nq} |w_{nq}^+|^2$  when the array is steered along  $(\theta_q, \varphi_q)$ , respectively. According to these definitions, the *FoV* of an antenna array can be identified as the angular range  $\Omega_{FoV}$  ( $\Omega_{FoV} \subset \Omega_{TOT}$ ,  $\Omega_{TOT} = \{(\theta_q, \varphi_q); q = 1, \dots, Q\}$ ) where the radiated power density in the scan direction  $(\theta_q, \varphi_q)$  is greater than a threshold  $\psi_{TH}$  (i.e.,  $\psi_q(\theta_q, \varphi_q) \geq \psi_{TH}$ ) and the total reflected power percentage is smaller than a target value  $\zeta_{TH}$  (i.e.,  $\zeta_q \leq \zeta_{TH}$ ). Mathematically, it turns out that  $(\theta_q, \varphi_q) \in \Omega_{FoV}$  if

$$\begin{aligned} \psi_q(\theta_q, \varphi_q) &\geq \psi_{TH} \\ \zeta_q &\leq \zeta_{TH}. \end{aligned} \quad (7)$$

In order to achieve wide scan performance (i.e., a wide *FoV*), *SoA* methods in the reference literature [3][5]-[13] require an  $ARL_{nq}$  almost independent on the angular direction (i.e.,  $ARL_{nq} \approx ARL_n$ ) and smaller than an application-defined threshold  $ARL_{TH}$  ( $ARL_n \leq ARL_{TH}$ ) by enforcing the condition  $|S_{nm}| \rightarrow 0$  ( $n = 1, \dots, N; m = 1, \dots, M; m \neq n$ ) to yield

$$\Gamma_n(\theta_q, \varphi_q) \approx S_{nn}. \quad (8)$$

Therefore, the condition  $ARL_n \leq ARL_{TH}$  is fulfilled by properly setting the descriptors of the elementary radiator,  $\underline{g}$ , so that  $|S_{nn}|^2 \leq ARL_{TH}$ , while the incident excitation coefficients  $\underline{w}_q^+$  are optimized to fulfill the requirements on the radiated power density along  $(\theta_q, \varphi_q)$ ,  $\psi_q(\theta_q, \varphi_q)$ .

Otherwise, the proposed approach leverages the observation that, according to (2), for a given matrix  $\mathcal{S}$  (i.e., resulting from the definition of the element geometries, physical properties, and positions), both the total reflected power percentage,  $\zeta_q$ , and the radiation properties of the array  $\mathbf{E}(\mathbf{r}|\underline{w}_q)$  (4) can be controlled by properly optimizing the excitations  $\underline{w}_q^+$  ( $q = 1, \dots, Q$ ) to maximize the *FoV* of the antenna array. Therefore, the design of the optimal excitations for

the  $q$ -th ( $q = 1, \dots, Q$ ) scan angle,  $\underline{w}_q^+ \big|_{opt}$ , is mathematically formulated as a multi-objective constrained optimization where  $\underline{w}_q^+ \big|_{opt}$  is the set of excitations  $\underline{w}_q^+$  that fulfils some feasibility conditions (i.e.,  $\underline{w}^+ \in \mathcal{W}$ ,  $\mathcal{W}$  being a set of requirements on the excitation coefficients such as constant magnitude, phase quantization, etc ...), while minimizing the  $T = 2$  objective functions coding the *FoV* condition (7)

$$\underline{w}_q^+ \big|_{opt} \triangleq \arg \left\{ \min_{\underline{w}_q^+} [\Phi_{REFL}(\underline{w}_q^+); \Phi_{RAD}(\underline{w}_q^+)] \right\}. \quad (9)$$

In (9), the first objective function  $\Phi_{REFL}$  coincides with the total reflected power percentage when the array is steered along  $(\theta_q, \varphi_q)$

$$\Phi_{REFL}(\underline{w}_q^+) \triangleq \zeta_q, \quad (10)$$

while the second one,  $\Phi_{RAD}$ , is defined as the inverse of the power density radiated along the  $q$ -th ( $q = 1, \dots, Q$ ) steering direction

$$\Phi_{RAD}(\underline{w}_q^+) = \frac{1}{\psi_q(\theta_q, \varphi_q)}. \quad (11)$$

As it can be noticed, the synthesis process at hand does not involve the geometrical descriptors of the array,  $\underline{g}$ , which are user-defined and *a-priori* set.

Since (9) codes a multi-objective optimization problem, which involves highly non-linear cost function terms, and the unknowns (i.e., magnitude/phase of the  $\underline{w}^+$  entries) are real-valued, a multi-objective steady-state evolutionary algorithm that uses  $\varepsilon$ -dominance archiving ( $\varepsilon$ -*MOEA*) to record a diverse set of Pareto optimal solutions has been adopted [22]-[24].

Unlike generational algorithms [25], the  $\varepsilon$ -*MOEA* evolves one solution at a time to ensure convergence and diversity throughout the optimization process [22]-[24]. For each  $q$ -th ( $q = 1, \dots, Q$ ) scan angle,  $(\theta_q, \varphi_q)$ , the following iterative procedure ( $c$  being the iteration index) is performed. At each  $c$ -th ( $c = 1, \dots, C$ ) iteration, both a variable-sized Pareto front  $\mathcal{A}_{cq}$  of  $A_{cq}$  solutions [ $\mathcal{A}_{cq} = \{\underline{w}_q^+ \big|_c^{(a)}; a = 1, \dots, A_{cq}\}$ ] and a fixed size population  $\mathcal{P}_{cq}$  of  $P$  individuals [ $\mathcal{P}_{cq} = \{\underline{w}_q^+ \big|_c^{(p)}; p = 1, \dots, P\}$ ] are evolved according to the  $\varepsilon$ -*MOEA* mutation, recombina-

tion, and selection operators with control parameters  $\underline{\varepsilon} = \{\varepsilon_1, \varepsilon_2\}$  [22]-[24]. At the convergence (i.e.,  $c = C$ ), a Pareto front of non-dominated excitation sets  $\mathcal{A}_{Cq}$  is outputted and the user identifies the optimal one according to a criterion based on either functional (i.e., a set of conditions on  $\Phi_{RAD}$  and/or  $\Phi_{REFL}$ ) or non-functional (e.g., costs, maintenance, etc ...) constraints.

Finally, the  $FoV$   $\Omega_{FoV}$  of the synthesized array (i.e.,  $\underline{W}^+ \Big|_{opt} = \left\{ \underline{w}_q^+ \Big|_{opt} ; q = 1, \dots, Q_{FoV} \right\}$ ) turns out to be the set of  $Q_{FoV}$  ( $Q_{FoV} \leq Q$ ) adjacent scan directions for which (7) holds true.

### 3 Numerical Results

This section is aimed at both illustrating the features of the proposed method and assessing its effectiveness also in comparison with state-of-the-art solutions.

The first numerical example deals with a linear array of  $N = 5$  equally-spaced by  $d = 0.47\lambda$  cavity-backed slot-fed microstrip antennas [Fig. 2(a)] printed on a Polyflon CuFlon substrate with thickness  $9 \times 10^{-3}$  [m]. Each radiator [Fig. 2(b)] has been modeled in Ansys HFSS [27] by choosing the following  $L = 7$  descriptors to operate at  $f = 2$  GHz:  $g_1 = 4.13 \times 10^{-2}$  [m],  $g_2 = 6.18 \times 10^{-2}$  [m],  $g_3 = 3.09 \times 10^{-2}$  [m],  $g_4 = 4.58 \times 10^{-2}$  [m],  $g_5 = 2.54 \times 10^{-3}$  [m],  $g_6 = 1.27 \times 10^{-2}$  [m], and  $g_7 = 4.63 \times 10^{-3}$  [m]. Moreover,  $\Omega_{FoV}$  has been defined by setting in (7)  $\zeta_{TH} = 10$  % and choosing  $\psi_{TH}$  so that the maximum array scan loss is  $-6$  [dB] (i.e.,  $\psi_{TH} = -6 + \psi_1(90, 0)$  [dB]). As for the array synthesis method, the requirement that no magnitude tapering is allowed (i.e.,  $|w_{nq}^+| = 1$ ,  $n = 1, \dots, N$  and  $q = 1, \dots, Q$ ), so that only the phases of the excitations are optimized ( $PO$ ), has been encoded into the feasibility set  $\mathcal{W}$  and the criterion for selecting the optimal trade-off array (i.e.,  $\underline{W}^+ \Big|_{opt}$ ) has been defined by setting  $\Phi_{RAD}^{PO} \equiv \Phi_{RAD}^{STD}$ ,  $\Phi_{RAD}^{STD}$  being (11) of the standard approach ( $STD$ ) where the excitation phases are computed with the analytic linear phase shifting rule [17]. Finally, the  $\varepsilon$ - $MOEA$  optimizer has been configured according to reference guidelines [22]-[24] by choosing the following setup:  $\{\varepsilon_1, \varepsilon_2\} = \{5 \times 10^{-3}, 2.5 \times 10^{-2}\}$ ,  $P = 50$ , and  $C = 1000$ .

In order to illustrate the features and the behavior of the proposed method for a generic  $q$ -th ( $q = 1, \dots, Q$ ) scan angle, Figure 2(c) shows the Pareto front  $\mathcal{A}_{Cq}$  when  $(\theta_q, \varphi_q) = (90, 52)$  [deg] ( $\rightarrow q = 53$ ). As it can be observed the  $PO$  Pareto front dominates the  $STD$  solution and the optimal trade-off array [i.e., the “green” cross in Fig. 2(c)] reduces the total reflected power percentage



from  $\zeta_q^{STD} = 24.6\%$  (i.e.,  $\Phi_{REFL}^{STD} = 0.246$ ) down to  $\zeta_q^{PO} = 8.9\%$  (i.e.,  $\Phi_{REFL}^{PO} = 0.089$ ), while keeping the same radiation performance (i.e.,  $\psi_q^{PO}(\theta_q, \varphi_q)|_{q=53} = \psi_q^{STD}(\theta_q, \varphi_q)|_{q=53} = 34.6$  [dBW/sterad]  $\rightarrow \Phi_{RAD} = 3.43 \times 10^{-4}$ ). The optimized excitations, which are reported in Fig. 3(a), turns out to be very similar, which implies an analogous architectural complexity, while the corresponding *ARL* values are mitigated with respect to the *STD* approach [ $ARL_{nq}^{PO} < ARL_{nq}^{STD}$ ,  $n = 1, \dots, N$  - Fig. 3(b)]. This latter outcome confirms that it is possible to indirectly control the *ARL* of a finite array by minimizing the total reflected power without reducing the radiated power along the steering direction as shown in Fig. 4.

The resume of the *PO* performance for the first test case is given in Fig. 5 where the plots of the radiated power density,  $\psi_q(\theta_q, \varphi_q)$  ( $q = 1, \dots, Q$ ;  $Q = 91$ ) [Fig. 5(a)], and the total reflected power percentage,  $\zeta_q$  ( $q = 1, \dots, Q$ ;  $Q = 91$ ) [Fig. 5(b)], are reported. As it can be inferred, the scan width of the finite array is enlarged of about 22 [deg] (i.e.,  $-42$  [deg]  $\leq \Omega_{FoV}^{STD} \leq 42$  [deg] vs.  $-53$  [deg]  $\leq \Omega_{FoV}^{PO} \leq 53$  [deg]), which corresponds to an increment of the field of view percentage  $\alpha_{FoV}$  ( $\alpha_{FoV} \triangleq \frac{Q_{FoV}}{Q}$ ) from  $\alpha_{FoV}^{STD} \approx 46\%$  up to  $\alpha_{FoV}^{PO} \approx 58\%$  ( $\rightarrow \Delta\alpha_{FoV} \approx 12\%$ ) and a maximum reduction of the reflected power within  $\Omega_{FoV}^{PO}$  that amounts to  $\Delta\zeta_{max}^{STD} = 15.7\%$  [ $\Delta\zeta_{max}^{STD} \triangleq \max_{q=1, \dots, Q_{FoV}}(\Delta\zeta_q^{STD})$  being  $\Delta\zeta_q^{STD} \triangleq \zeta_q^{STD} - \zeta_q^{PO}$ ].

The applicability of the considered approach to wider linear arrays is assessed next by considering a larger arrangement with  $N = 16$  elements [Fig. 6(a)]. While there is still a widening of the *FoV* [Figs. 6(b)-6(c)], the improvement with respect to the *STD* layout is here smaller ( $\Delta\alpha_{FoV} \approx 4\%$   $\rightarrow \Delta\Omega_{FoV} \approx 8$  [deg]) since the efficiency of the proposed method in balancing the input power among the array elements is vanifed by the uniform coupling among the majority of them.

The third test case is concerned with planar architectures. Towards this end, a planar  $N = 4 \times 4$  arrangement of radiators as in Fig. 2(a) has been considered (Fig. 7 -  $d_x = d_y = 0.47\lambda$ ) and the results from the *STD* and the *PO* syntheses are summarized in Fig. 8 by showing the color maps of  $\psi_q(\theta_q, \varphi_q)$  ( $q = 1, \dots, Q$ ;  $Q = 361$ ) [Figs. 8(a)-8(b)] and  $\zeta_q$  ( $q = 1, \dots, Q$ ;  $Q = 361$ ) [Figs. 8(c)-8(d)]. As expected, Figs. 8(a)-8(b) are almost identical by definition since the criterion for selecting the “optimal” trade-off solution forces the condition  $\Phi_{RAD}^{PO} \approx \Phi_{RAD}^{STD}$ . Otherwise, the advantage of the *PO* approach is evident when comparing Fig. 8(c) and Fig. 8(d) and

it is further highlighted in Fig. 8(e) where the reduction of the total reflected power,  $\Delta\zeta_q^{STD}$  ( $q = 1, \dots, Q$ ;  $Q = 361$ ) is reported,  $\Delta\zeta_{max}$  being equal to  $\Delta\zeta_{max} \approx 8\%$ . Therefore, the main outcome (i.e., the scanning performance of the finite array) is that the *PO* widens the field of view percentage from  $\alpha_{FoV}^{STD} \approx 40\%$  [Fig. 9(a)] up to  $\alpha_{FoV}^{PO} \approx 49\%$  [Fig. 9(b)] ( $\rightarrow \Delta\alpha_{FoV} \approx 9\%$ ).

The final numerical experiment is aimed at further assessing the *PO*-based solutions also against state-of-the-art wide scan layouts [28]. Accordingly, a planar arrangement of  $N = 8 \times 8$  ( $d_x = 0.42\lambda$ ,  $d_y = 0.43\lambda$ ) identical parasitic pixel layer-based E-shaped radiators [28] operating at  $f = 5.2\text{GHz}$  has been numerically modeled in Ansys HFSS (Fig. 10).

For comparison purposes, the plots of both the radiated power density and the total reflected power along the cut  $\varphi_q = 0$  [deg] are shown in Fig. 11 where the values in Tab. I [28] are reported, as well. Once again the *PO* array outperforms the *STD* one yielding on the  $\varphi_q = 0$  [deg] plane an improvement of the *FoV* of about  $\Delta\alpha_{FoV} \approx 13.2\%$  ( $\alpha_{FoV}^{STD} \approx 35.4\%$  vs.  $\alpha_{FoV}^{PO} \approx 48.6\%$  [Figs. 11(a)-11(b)]), while it turns out to be  $\Delta\alpha_{FoV} \approx 22.6\%$  in the whole angular range [Fig. 12(a) vs. Fig. 12(b)].

The *PO* layout is also better than that in [28] in terms of  $\psi_q(\theta_q, 0)$  and  $\zeta_q$  ( $q = 1, \dots, Q$ ;  $Q = 37$ ) at the available angular samples (i.e.,  $\theta_4 = -75$  [deg],  $\theta_8 = -55$  [deg],  $\theta_{30} = 55$  [deg], and  $\theta_{34} = 75$  [deg]) since  $2.49$  [dB]  $\leq \Delta\psi_q^{[Cheng2017]}(\theta_q, 0) \leq 18.35$  [dB] ( $\Delta\psi_q^{[Cheng2017]}(\theta_q, \varphi_q) \triangleq \psi_q^{PO}(\theta_q, \varphi_q) - \psi_q^{[Cheng2017]}(\theta_q, \varphi_q)$  [dB]) and  $8.8\%$   $\leq \Delta\zeta_q^{[Cheng2017]} \leq 24.64\%$  in Tab. I. For fairness, the comparison has been also carried out by considering the figures-of-merit optimized in [28] and the outcomes are summarized in Tab. II where  $SLL_q$ ,  $G_q$ , and  $\Delta\Theta_q$  are the normalized sidelobe level ( $SLL_q \triangleq \frac{\max_{(\theta, \varphi) \notin ML} \psi_q(\theta, \varphi)}{\max_{(\theta, \varphi)} \psi_q(\theta, \varphi)}$ ,  $ML$  being the main-lobe region), the array gain ( $G_q \triangleq 4\pi \frac{\max_{(\theta, \varphi)} \psi_q(\theta, \varphi)}{\mathbb{P}_{IN}}$ ), and the scan angle error ( $\Delta\Theta_q \triangleq \theta_q - \arg \{ \max_{(\theta, \varphi)} \psi_q(\theta, \varphi) \}$ ), respectively. As it can be noticed (Tab. II), the values for the two layouts are quite similar (i.e.,  $-3.66$  [dB]  $\leq \Delta SLL_q^{[Cheng2017]} \leq -0.23$  [dB],  $0.01$  [dB]  $\leq \Delta G_q^{[Cheng2017]} \leq 0.50$  [dB], and  $-0.48$  [deg]  $\leq \Delta\Theta_q^{[Cheng2017]} \leq 4.12$  [deg]).

Finally, Figure 13 gives the color level maps of the *ARL* of the  $N = 8 \times 8$  array elements when  $(\theta_q, \varphi_q) = (-75, 0)$  [deg] (i.e.,  $q = 4$ ),  $ARL_{nq}$  ( $n = 1, \dots, N$ ), for the *PO* [Fig. 13(a)], the *SoA* [28] [Fig. 13(b)], and the *STD* [Fig. 13(c)] layouts. One can observe that generally

$ARL_{nq}^{PO} < ARL_{TH}$  ( $n = 1, \dots, N; q = 4$ ),  $ARL_{TH} = -10$  [dB]. This outcome further assesses the capability of the *PO*-based synthesis to indirectly control the *ARL* of a finite array by minimizing the total reflected power without reducing the radiated power along the steering direction. Moreover, the condition  $ARL_{nq}^{PO} < ARL_{nq}^{[Cheng\ 2017]}$  ( $q = 4$ ) holds true in several  $n$ -th ( $n = 1, \dots, N$ ) radiating elements [Fig. 13(a) vs. Fig. 13(b)], while  $ARL_{nq}^{[Cheng\ 2017]} \approx ARL_{nq}^{STD}$  ( $n = 1, \dots, N; q = 4$ ).

## 4 Conclusions and Observations

The synthesis of the excitations of antenna arrays to achieve wide-angle scanning features [i.e., a wide field-of-view (*FoV*)] with minimum reflected power has been addressed. Towards this end, an innovative methodology has been proposed by formulating the array synthesis as a multi-objective problem where, for each scan angle, both the radiated power density in the scan direction and the total reflected power are accounted for by including the finite array coupling in the design process (i.e., no periodicity approximation is employed). The effectiveness of the approach has been assessed with a selected set of numerical test cases by also proving the possibility to indirectly control the *ARL* of finite arrays.

The main outcomes from the numerical validation, which has been carried out with a commercial full-wave software [27] to have a faithful modelling of all the electromagnetic interactions, can be summarized as follows:

- the implemented design concept outperforms the standard linear phase shifting technique [17] in yielding wide-angle scanning arrays regardless of the frequency, the radiating elements, and the array arrangement (i.e., linear or planar);
- the *PO*-based synthesis method allows one to enhance the *FoV* of finite antenna arrays without modifying the antenna architecture, thus it can be applied to upgrade existing arrays;
- the multi-objective design process provides the user with a multiplicity of trade-off Pareto-front solutions, thus the possibility of choosing an optimal one depending on an application-

driven criterion based on either functional or non-functional (e.g., costs, maintenance, etc...) constraints.

Future works, beyond the scope of this manuscript, will be aimed at extending the proposed methodology to conformal structures.

## Acknowledgements

This work benefited from the networking activities carried out within the project DICAM-EXC (Departments of Excellence 2023-2027, grant L232/2016) funded by the Italian Ministry of Education, Universities and Research (MUR), the Project "Smart ElectroMagnetic Environment in TrentiNo - SEME@TN" funded by the Autonomous Province of Trento (CUP: C63C22000720003), the Project "AURORA - Smart Materials for Ubiquitous Energy Harvesting, Storage, and Delivery in Next Generation Sustainable Environments" funded by the Italian Ministry for Universities and Research within the PRIN-PNRR 2022 Program, and the following projects funded by the European Union - NextGenerationEU within the PNRR Program: Project "ICSC National Centre for HPC, Big Data and Quantum Computing (CN HPC)" (CUP: E63C22000970007), Project "Telecommunications of the Future (PE00000001 - program "RESTART", Structural Project 6GWINET)" (CUP: D43C22003080001), Project "INSIDE-NEXT - Indoor Smart Illuminator for Device Energization and Next-Generation Communications" (CUP: E53D23000990001), and Project "Telecommunications of the Future (PE00000001 - program "RESTART", Focused Project MOSS)" (CUP: J33C22002880001). A. Massa wishes to thank E. Vico for her never-ending inspiration, support, guidance, and help.

## References

- [1] J. S. Herd and M. D. Conway, "The evolution to modern phased array architectures," *Proc. IEEE*, vol. 104, no. 3, pp. 519-529, Mar. 2016.

- [2] S. Gao, Y. J. Guo, S. A. Safavi-Naeini, W. Hong, and X. -X. Yang, "Guest Editorial: Low-Cost Wide-Angle Beam-Scanning Antennas," *IEEE Trans. Antennas Propag.*, vol. 70, no. 9, pp. 7378-7383, Sep. 2022.
- [3] G. Oliveri, M. Salucci, R. Lombardi, R. Flamini, C. Mazzucco, S. Verzura, and A. Massa, "Wide-angle impedance matching layer-enhanced dual-polarization sub-6 GHz wide-scan array for next-generation base stations," *IEEE Trans. Antennas Propag.*, vol. 70, no. 7, pp. 5506-5520, Jul. 2022.
- [4] R. C. Hansen, *Phased Array Antennas*, John Wiley & Sons, Inc., 2009.
- [5] S. E. Valavan, D. Tran, A. G. Yarovoy, and A. G. Roederer, "Dual-band wide-angle scanning planar phased array in X/Ku-bands," *IEEE Trans. Antennas Propag.*, vol. 62, no. 5, pp. 2514-2521, May 2014.
- [6] S. E. Valavan, D. Tran, A. G. Yarovoy and A. G. Roederer, "Planar dual-band wide-scan phased array in X-band," *IEEE Trans. Antennas Propag.*, vol. 62, no. 10, pp. 5370-5375, Oct. 2014.
- [7] C. Liu, S. Xiao, and X. Zhang, "A compact, low-profile wire antenna applied to wide-angle scanning phased array," *IEEE Antennas Wireless Propag. Lett.*, vol. 17, no. 3, pp. 389-392, Mar. 2018.
- [8] R. Xia, S. Qu, X. Bai, Q. Jiang, S. Yang, and Z. Nie, "Experimental investigation of wide-angle impedance matching of phased array using overlapped feeding network," *IEEE Antennas Wireless Propag. Lett.*, vol. 13, pp. 1284-1287, 2014.
- [9] R. Xia, S. Qu, P. Li, D. Yang, S. Yang, and Z. Nie, "Wide-angle scanning phased array using an efficient decoupling network," *IEEE Trans. Antennas Propag.*, vol. 63, no. 11, pp. 5161-5165, Nov. 2015.
- [10] S. Sajuyigbe, M. Ross, P. Geren, S. A. Cummer, M. H. Tanielian, and D. R. Smith, "Wide angle impedance matching metamaterials for waveguide-fed phased-array antennas," *IET Microw. Antennas Propag.*, vol. 4, no. 8, pp. 1063-1072, Aug. 2010.

- [11] G. Oliveri, F. Viani, N. Anselmi, and A. Massa, "Synthesis of multilayer WAIM coatings for planar-phased arrays within the System-by-Design framework," *IEEE Trans. Antennas Propag.*, vol. 63, no. 6, pp. 2482-2496, Jun. 2015.
- [12] G. Oliveri, M. Salucci, N. Anselmi, and A. Massa, "Multiscale System-by-Design synthesis of printed WAIMs for waveguide array enhancement," *IEEE J. Multisc. Multiphys. Comput. Techn.*, vol. 2, pp. 84-96, 2017.
- [13] G. Oliveri, A. Polo, M. Salucci, G. Gottardi, and A. Massa, "SbD-based synthesis of low-profile WAIM superstrates for printed patch arrays," *IEEE Trans. Antennas Propag.*, vol. 69, no. 7, pp. 3849-3862, Jul. 2021.
- [14] P. Hannan, D. Lerner, and G. Knittel, "Impedance matching a phased-array antenna over wide scan angles by connecting circuits," *IEEE Trans. Antennas Propag.*, vol. 13, no. 1, pp. 28-34, Jan. 1965.
- [15] E. G. Magill and H. A. Wheeler, "Wide-Angle impedance matching of a planar array antenna by a dielectric sheet", *IEEE Trans. Antennas Propag.*, vol. AP-14, no. 1, pp. 49-53, Jan. 1966.
- [16] D. M. Pozar, "The active element pattern," *IEEE Transactions on Antennas and Propagation*, vol. 42, no. 8, pp. 1176-1178, Aug. 1994.
- [17] R. J. Mailloux, *Phased Array Antenna Handbook*, 2nd Ed. Norwood, MA, USA: Artech House, 2005.
- [18] G. Oliveri, G. Gottardi, and A. Massa, "A new meta-paradigm for the synthesis of antenna arrays for future wireless communications," *IEEE Trans. Antennas Propag.*, vol. 67, no. 6, pp. 3774-3788, Jun. 2019.
- [19] G. Oliveri, G. Gottardi, N. Anselmi, and A. Massa, "Capacity-driven low-interference fast beam synthesis for next generation base stations," *IEEE Trans. Antennas Propag.*, vol. 70, no. 6, pp. 4472-4484, Jun. 2022.

- [20] D. M. Pozar, "A relation between the active input impedance and the active element pattern of a phased array," *IEEE Trans. Antennas Propag.*, vol. 51, no. 9, pp. 2486-2489, Sep. 2003.
- [21] C. A. Balanis, *Advanced Engineering Electromagnetics*, New York, NY: John Wiley and Sons, 1989.
- [22] K. Deb, M. Mohan, and S. Mishra "A fast multi-objective evolutionary algorithm for finding well-spread Pareto-optimal solutions," *KanGAL Report No 2003002*, Feb. 2003.
- [23] M. Laumanns, L. Thiele, K. Deb, and E. Zitzler, "Combining convergence and diversity in evolutionary multiobjective optimization," *Evolution. Comput.*, vol. 10, no. 3, pp. 263-282, Sep. 2002.
- [24] P. Rosatti, M. Salucci, L. Poli, and A. Massa, "Multiobjective System-by-Design for mm-Wave automotive radar antennas," *IEEE Trans. Antennas Propag.*, vol. 71, no. 4, pp. 2958-2973, Apr. 2023.
- [25] P. Rocca, M. Benedetti, M. Donelli, D. Franceschini, and A. Massa, "Evolutionary optimization as applied to inverse problems," *Inv. Probl.*, vol. 25, art no. 123003, pp. 1-41, Dec. 2009.
- [26] W.Y. Chiu, G. G. Yen, and T. K. Juan, "Minimum Manhattan distance approach to multiple criteria decision making in multiobjective optimization problems," *IEEE Trans. Evolution. Computat.*, vol. 20, no. 6, pp. 972-985, Dec. 2016.
- [27] ANSYS Electromagnetics Suite - HFSS (2021). ANSYS, Inc.
- [28] Y. Cheng, X. Ding, W. Shao, M. Yu, and B. Wang, "2-D Planar wide-angle scanning-phased array based on wide-beam elements," *IEEE Antennas Wireless Propag. Lett.*, vol. 16, pp. 876-879, 2017.

## FIGURE CAPTIONS

- **Figure 1.** *Problem geometry.* Sketch of the reference phased array layout.
- **Figure 2.** *Slot-fed patch linear array* ( $N = 5$ ,  $f = 2$  [GHz],  $d = 0.47\lambda$ ) - Sketch of (a) the geometry of array element and (b) the HFSS model of the array, and plot of the Pareto-optimal solutions when  $(\theta_q, \varphi_q) = (90, 52)$  [deg].
- **Figure 3.** *Slot-fed patch linear array* ( $N = 5$ ,  $f = 2$  [GHz],  $d = 0.47\lambda$ ,  $q = 53$ ,  $(\theta_q, \varphi_q) = (90, 52)$  [deg]) - Plots of (a)  $\angle w_{nq}^+$  and (b)  $ARL_{nq}$ ,  $n = 1, \dots, N$ .
- **Figure 4.** *Slot-fed patch linear array* ( $N = 5$ ,  $f = 2$  [GHz],  $d = 0.47\lambda$ ,  $q = 53$ ,  $(\theta_q, \varphi_q) = (90, 52)$  [deg],  $\theta = 90$  [deg]) - Plot of  $\psi_q(\theta, \varphi)$ .
- **Figure 5.** *Slot-fed patch linear array* ( $N = 5$ ,  $f = 2$  [GHz],  $d = 0.47\lambda$ ,  $\theta_q = 90$  [deg]) - Plots of (a)  $\psi_q(\theta_q, \varphi_q)$  and (b)  $\zeta_q$  versus  $\varphi_q$  ( $q = 1, \dots, Q$ ;  $Q = 91$ ).
- **Figure 6.** *Slot-fed patch linear array* ( $N = 16$ ,  $f = 2$  [GHz],  $d = 0.47\lambda$ ,  $\theta_q = 90$  [deg]) - Sketch of (a) the HFSS model of the array and plots of (b)  $\psi_q(\theta_q, \varphi_q)$ , and (c)  $\zeta_q$  versus  $\varphi_q$  ( $q = 1, \dots, Q$ ;  $Q = 91$ ).
- **Figure 7.** *Slot-fed patch planar array* ( $N = 4 \times 4$ ,  $f = 2$  [GHz],  $d_x = d_y = 0.47\lambda$ ) - Sketch of the HFSS model of the array.
- **Figure 8.** *Slot-fed patch planar array* ( $N = 4 \times 4$ ,  $f = 2$  [GHz],  $d_x = d_y = 0.47\lambda$ ) - Plots of (a)(b)  $\psi_q(\theta_q, \varphi_q)$ , (c)(d)  $\zeta_q$ , and (e)  $\Delta\zeta_q^{STD}$  ( $q = 1, \dots, Q$ ;  $Q = 361$ ).
- **Figure 9.** *Slot-fed patch planar array* ( $N = 4 \times 4$ ,  $f = 2$  [GHz],  $d_x = d_y = 0.47\lambda$ ) - Plot of  $\Omega^{FoV}$  (in green) of (a) the *STD* and (b) the *PO* arrays.
- **Figure 10.** *Pin-fed E-patch planar array* ( $N = 8 \times 8$ ,  $f = 5.2$  [GHz],  $d_x = 0.42\lambda$ ,  $d_y = 0.43\lambda$ ) - Sketch of the HFSS model of the array.
- **Figure 11.** *Pin-fed E-patch planar array* ( $N = 8 \times 8$ ,  $f = 5.2$  [GHz],  $d_x = 0.42\lambda$ ,  $d_y = 0.43\lambda$ ,  $\varphi_q = 0$  [deg]) - Plots of (a)  $\psi_q(\theta_q, \varphi_q)$  and (b)  $\zeta_q$  versus  $\theta_q$  ( $q = 1, \dots, Q$ ;  $Q = 37$ ).



- **Figure 12.** *Pin-fed E-patch planar array* ( $N = 8 \times 8$ ,  $f = 5.2$  [GHz],  $d_x = 0.42\lambda$ ,  $d_y = 0.43\lambda$ ) - Plot of  $\Omega^{FoV}$  (in green) of (a) the *STD* and (b) the *PO* arrays.
- **Figure 13.** *Pin-fed E-patch planar array* ( $N = 8 \times 8$ ,  $f = 5.2$  [GHz],  $d_x = 0.42\lambda$ ,  $d_y = 0.43\lambda$ ,  $q = 4$ ,  $(\theta_q, \varphi_q) = (-75, 0)$  [deg]) - Plots of  $ARL_{nq}$ ,  $n = 1, \dots, N$  of (a) *PO*, (b) *SoA* [28], and (c) the *STD* arrays.

## TABLE CAPTIONS

- **Table I.** *Pin-fed E-patch planar array* ( $N = 8 \times 8$ ,  $f = 5.2$  [GHz],  $d_x = 0.42\lambda$ ,  $d_y = 0.43\lambda$ ,  $\varphi_q = 0$  [deg]) - Performance indexes.
- **Table II.** *Pin-fed E-patch planar array* ( $N = 8 \times 8$ ,  $f = 5.2$  [GHz],  $d_x = 0.42\lambda$ ,  $d_y = 0.43\lambda$ ,  $\varphi_q = 0$  [deg]) - Performance indexes in [28].

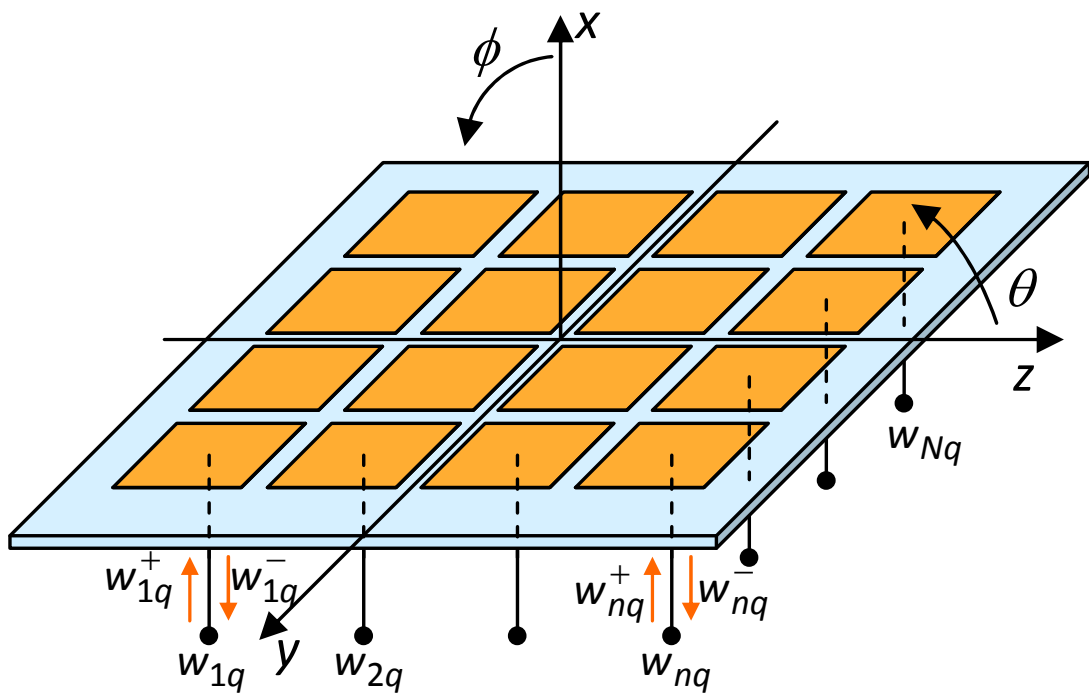
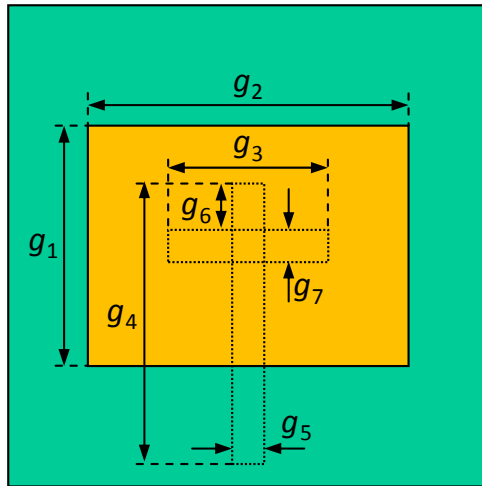
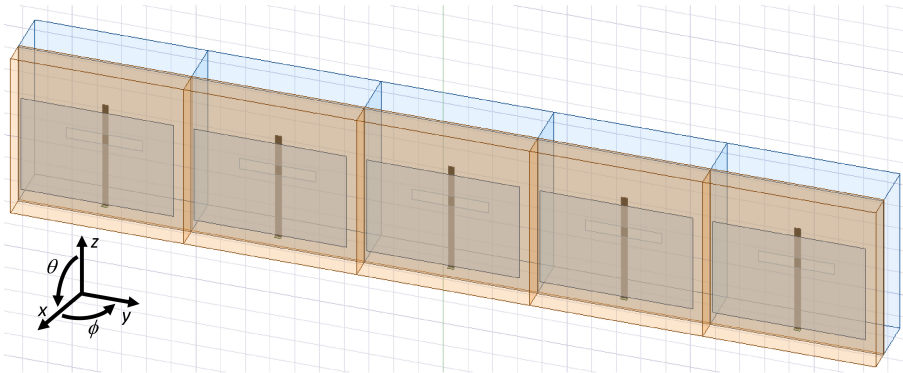


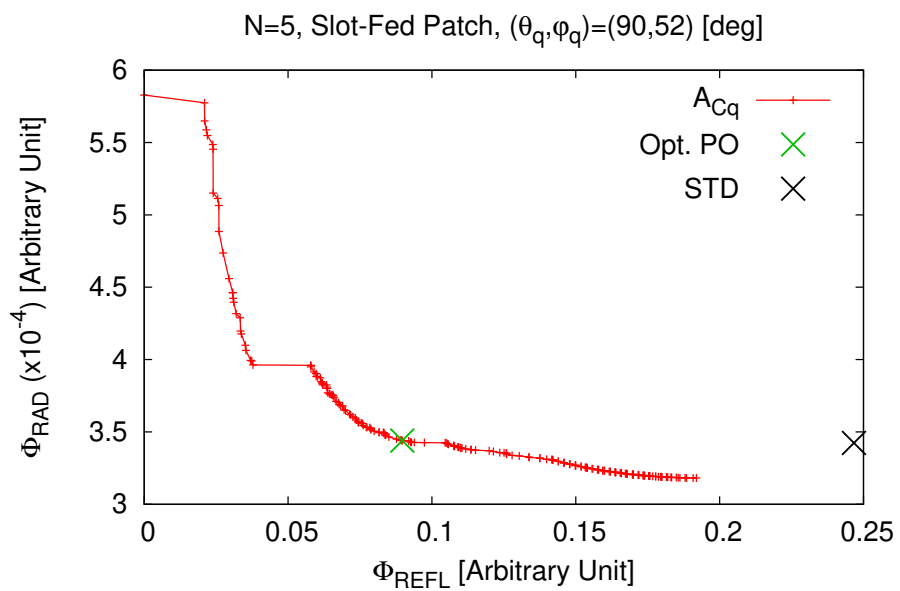
Fig. 1 - P. Rosatti *et al.*, “Synthesis of Wide-Angle Scanning Arrays ...”



(a)

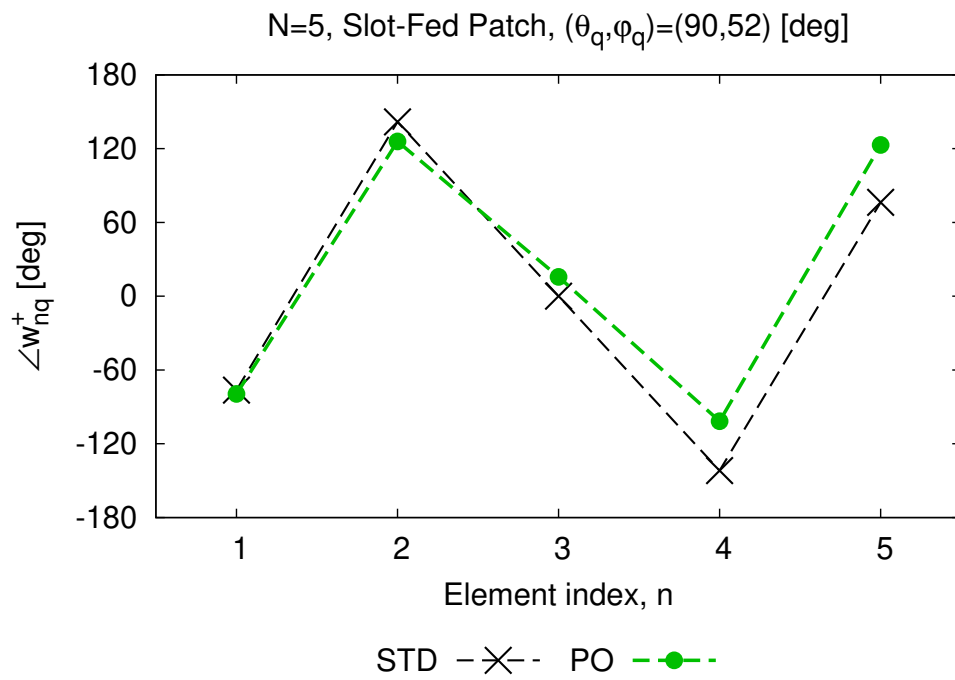


(b)

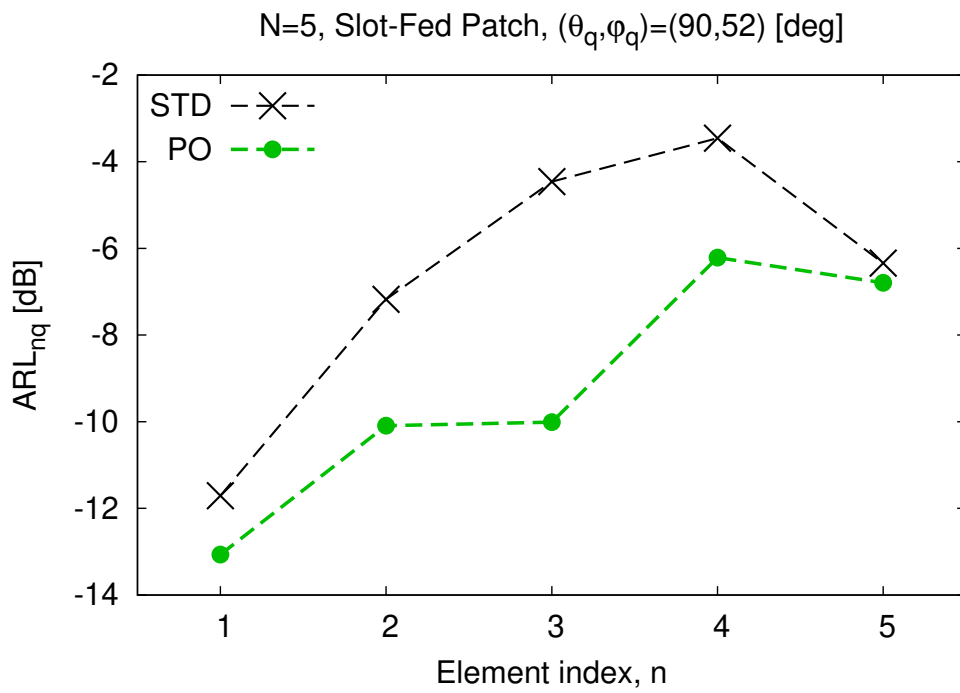


(c)

Fig. 2 - P. Rosatti *et al.*, “Synthesis of Wide-Angle Scanning Arrays ...”



(a)



(b)

**Fig. 3 - P. Rosatti *et al.*, “Synthesis of Wide-Angle Scanning Arrays ...”**

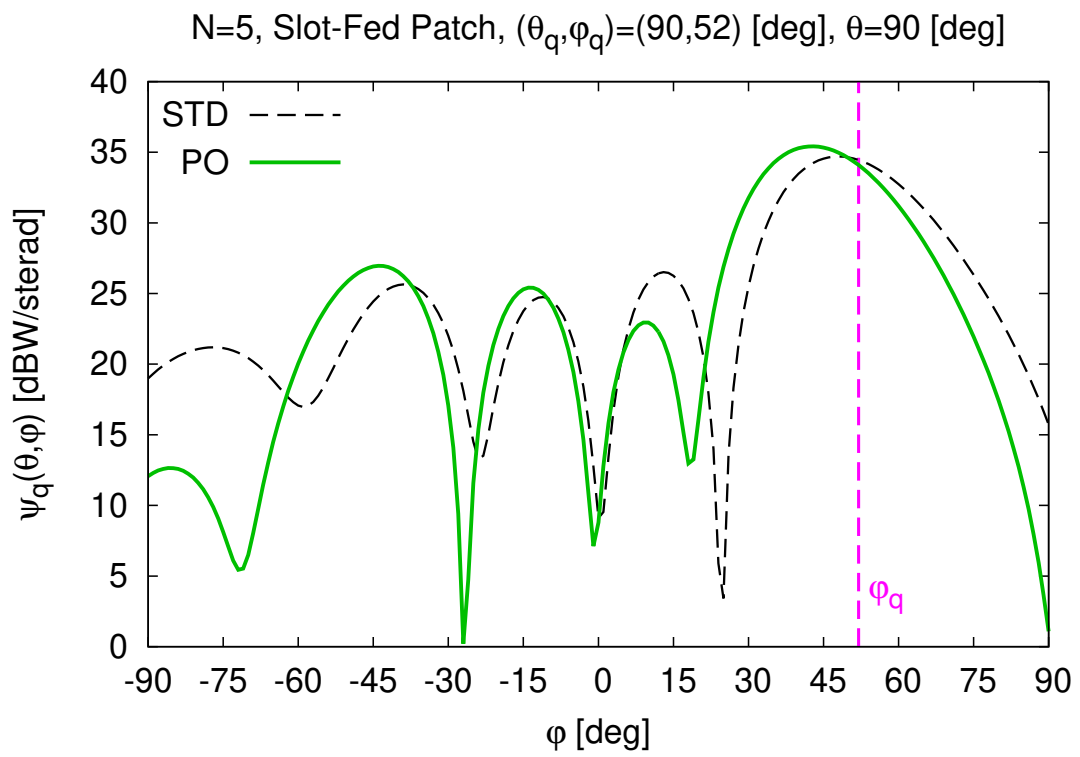
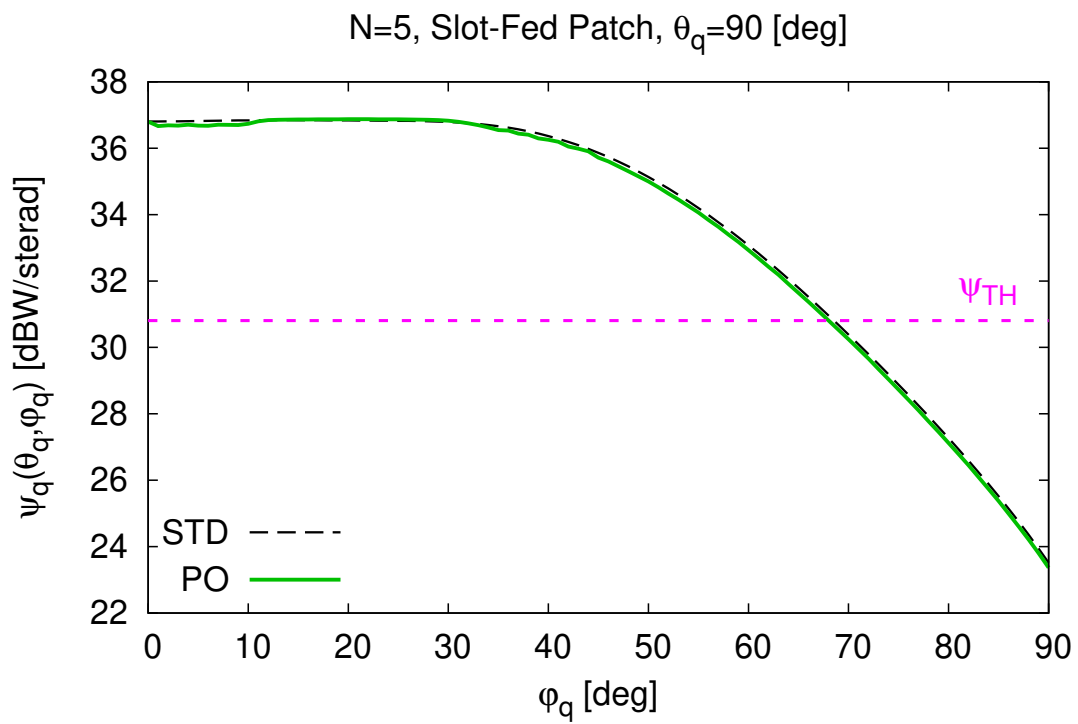
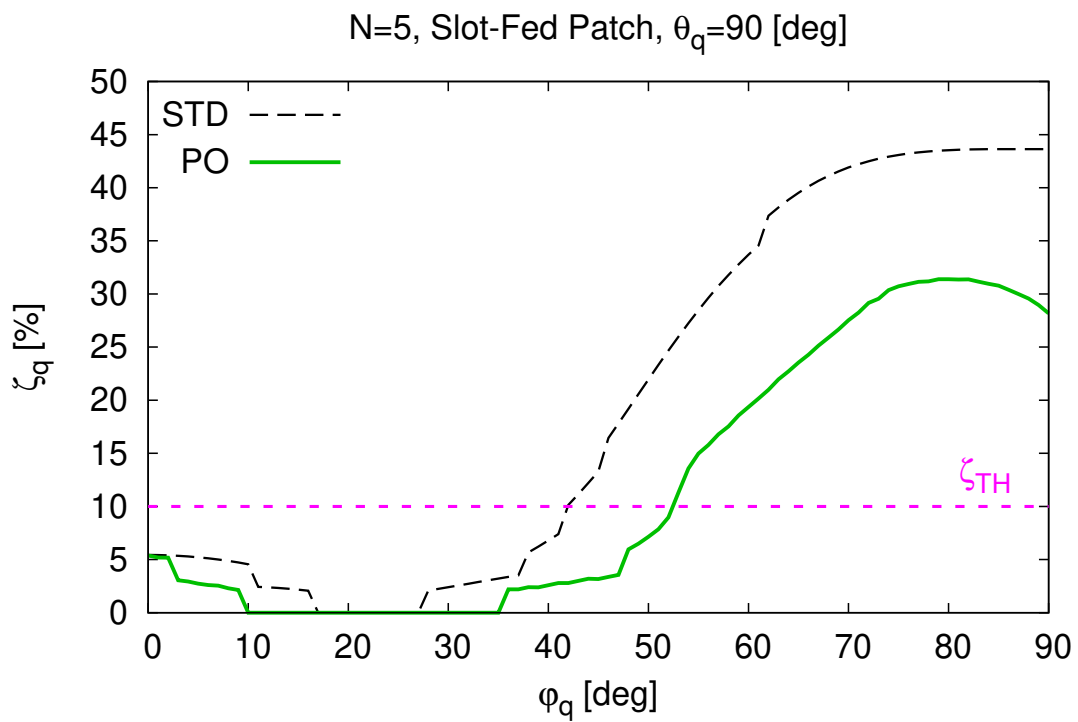


**Fig. 4 - P. Rosatti *et al.*, “Synthesis of Wide-Angle Scanning Arrays ...”**

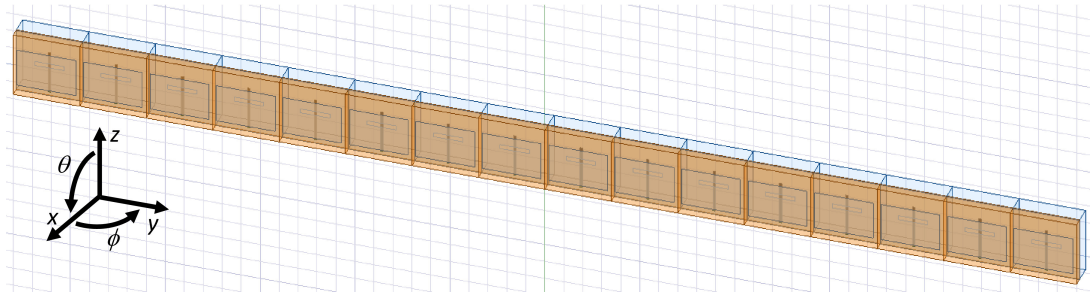


(a)

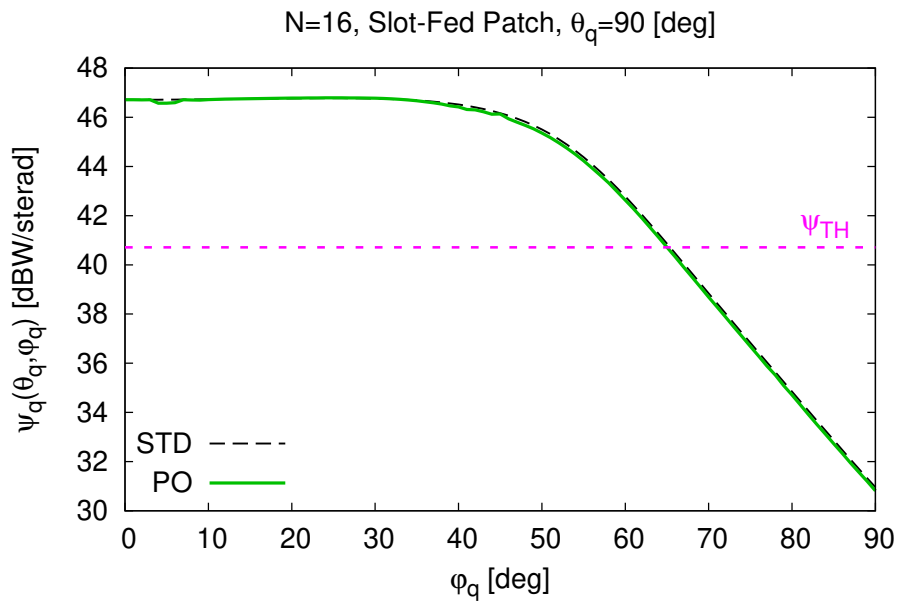


(b)

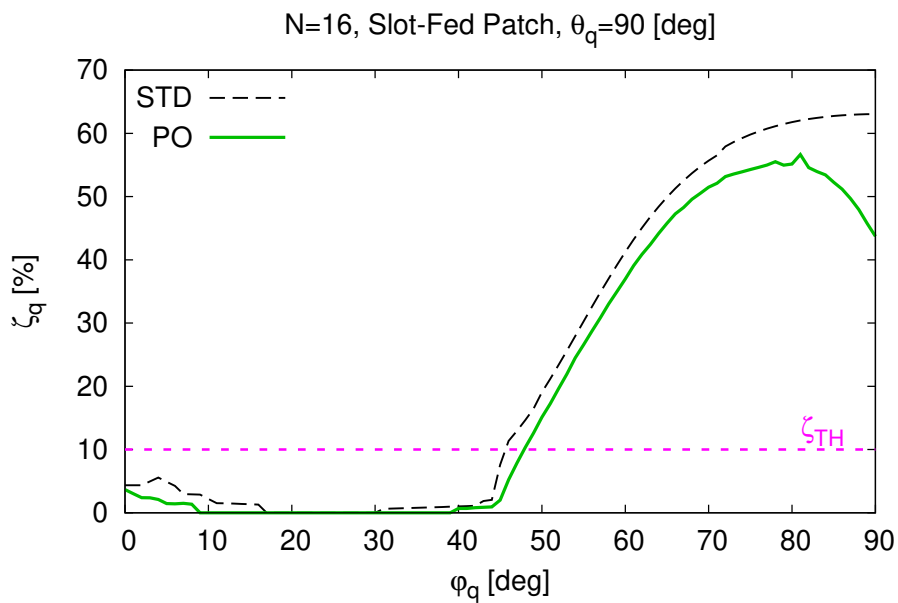
**Fig. 5 - P. Rosatti *et al.*, “Synthesis of Wide-Angle Scanning Arrays ...”**



(a)



(b)



(c)

Fig. 6 - P. Rosatti *et al.*, "Synthesis of Wide-Angle Scanning Arrays ..."

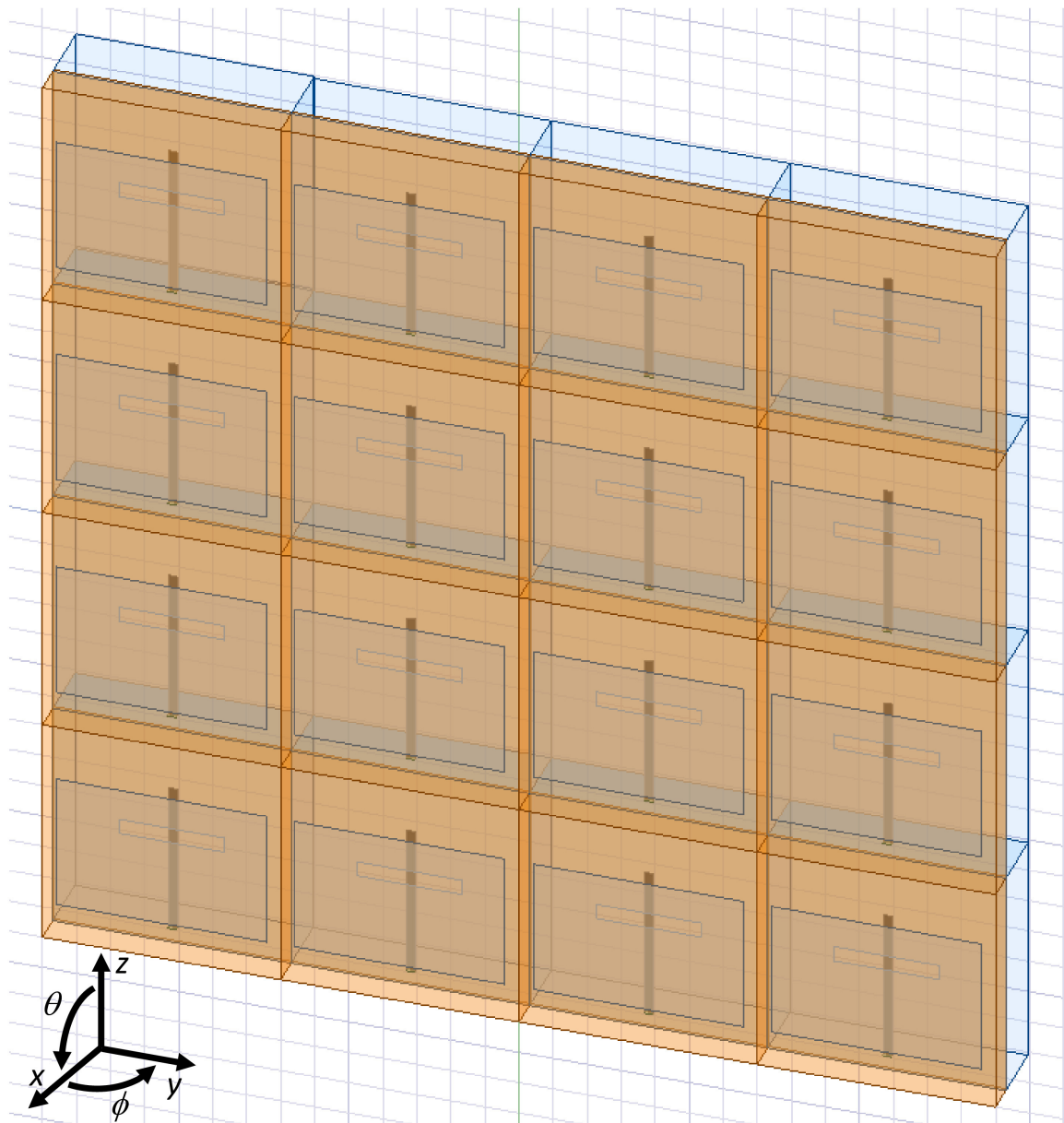


Fig. 7 - P. Rosatti *et al.*, "Synthesis of Wide-Angle Scanning Arrays ..."



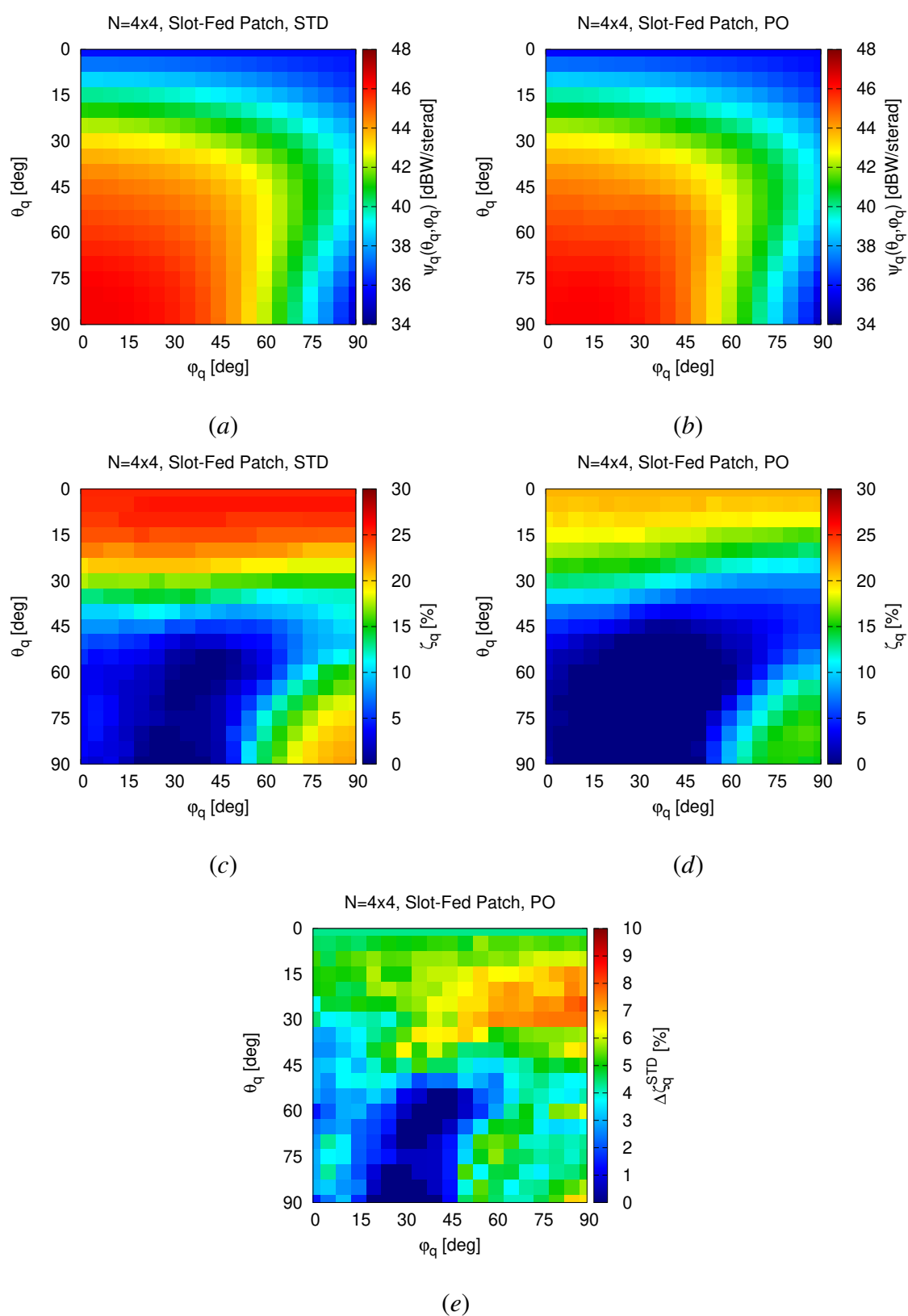
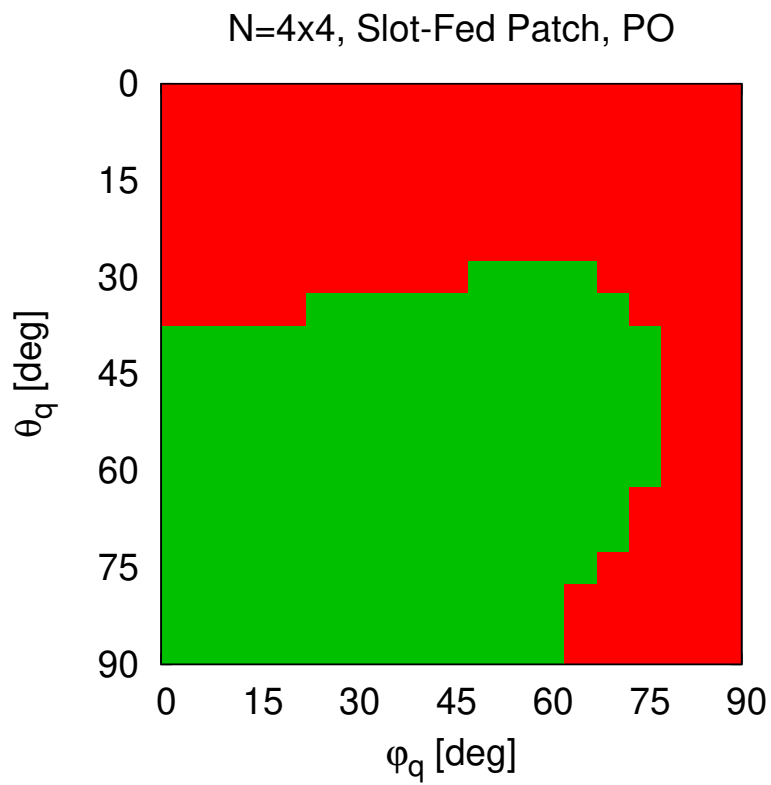
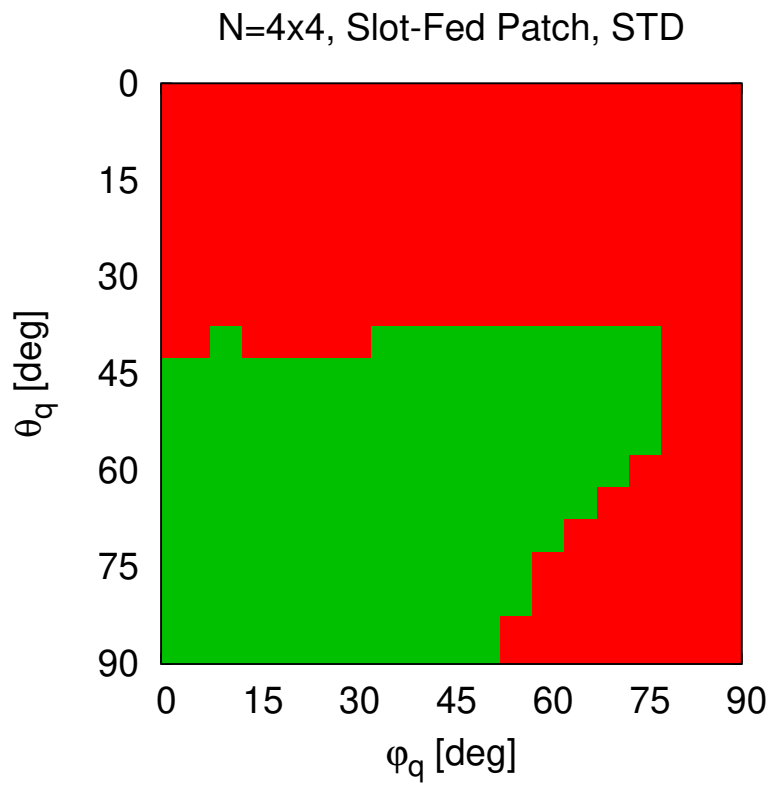


Fig. 8 - P. Rosatti *et al.*, “Synthesis of Wide-Angle Scanning Arrays ...”



**Fig. 9** - P. Rosatti *et al.*, “Synthesis of Wide-Angle Scanning Arrays ...”

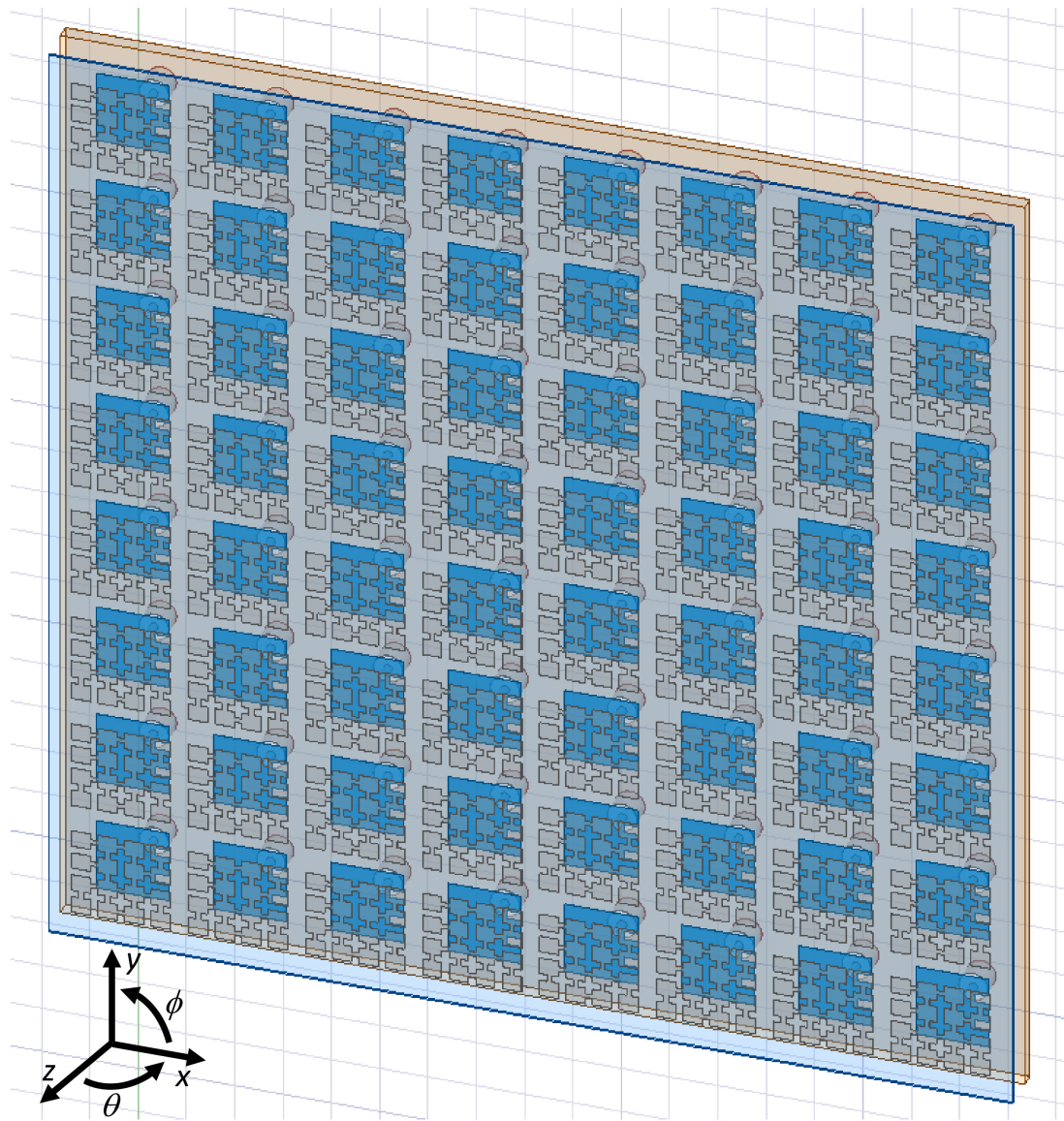
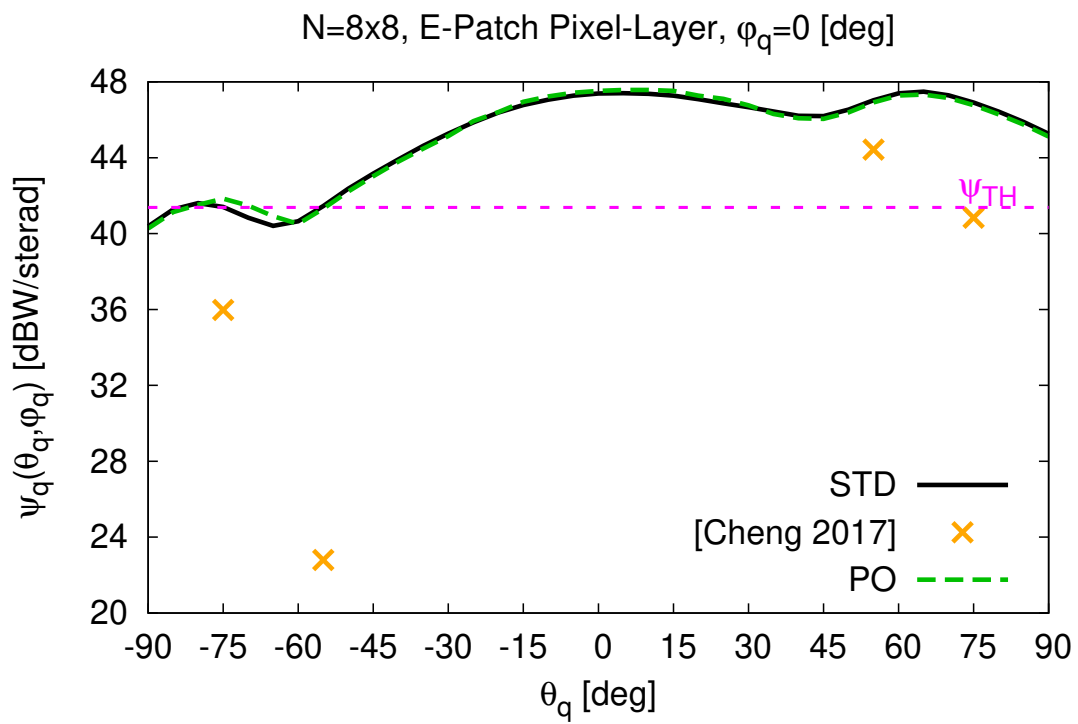
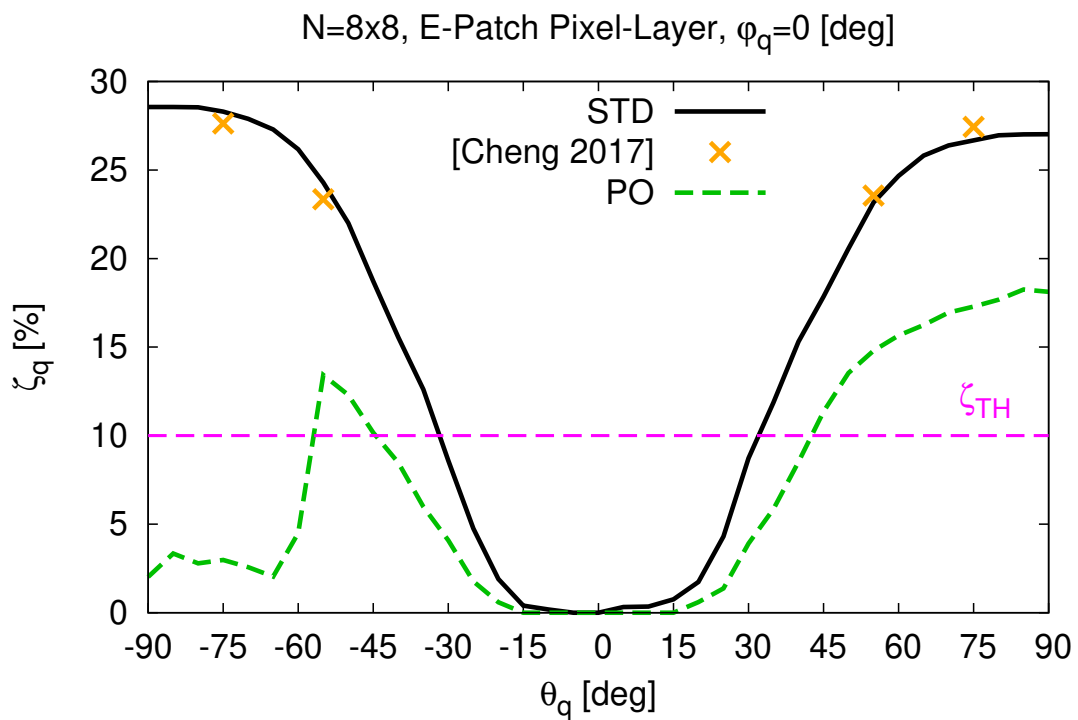


Fig. 10 - P. Rosatti *et al.*, “Synthesis of Wide-Angle Scanning Arrays ...”



(a)



(b)

Fig. 11 - P. Rosatti *et al.*, “Synthesis of Wide-Angle Scanning Arrays ...”

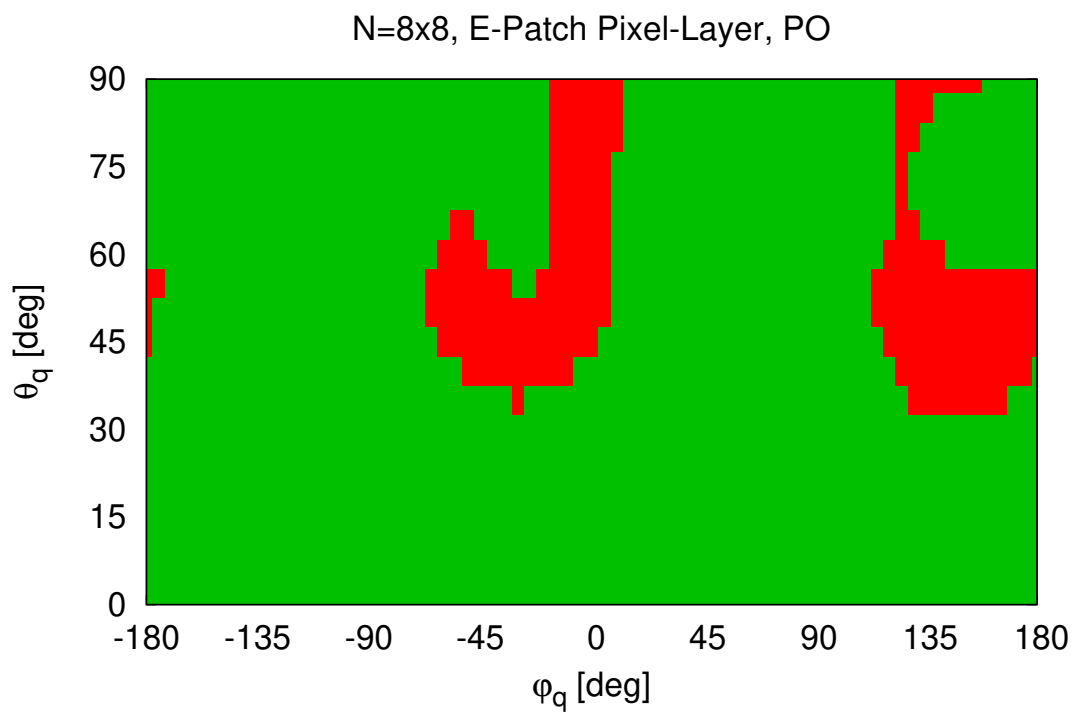
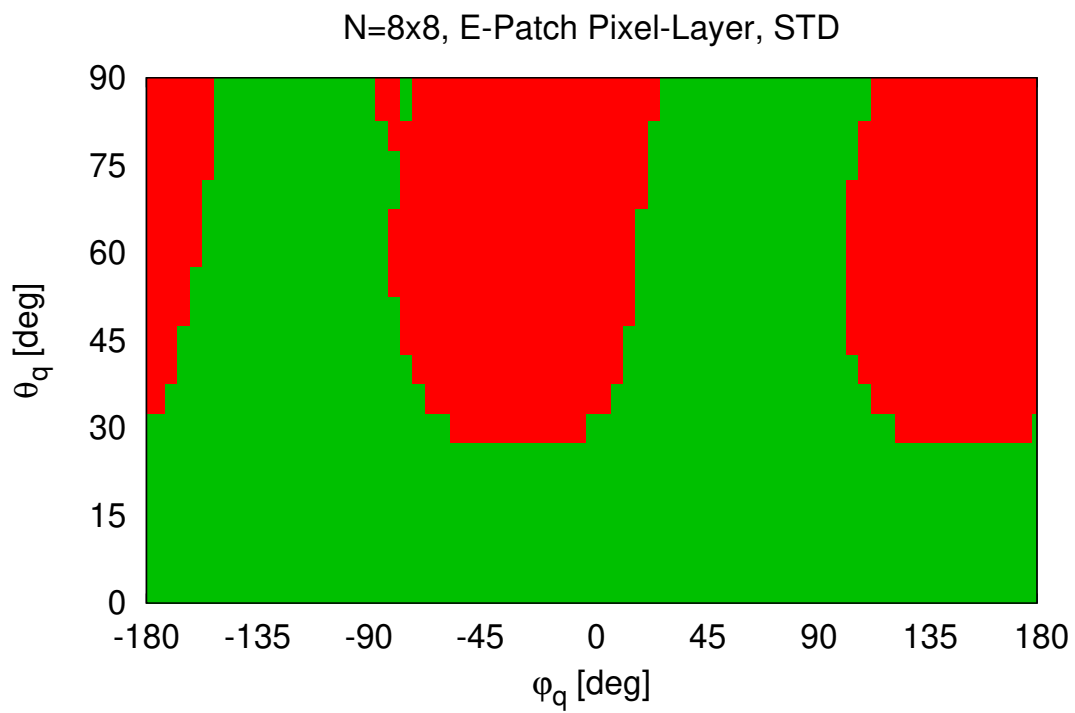
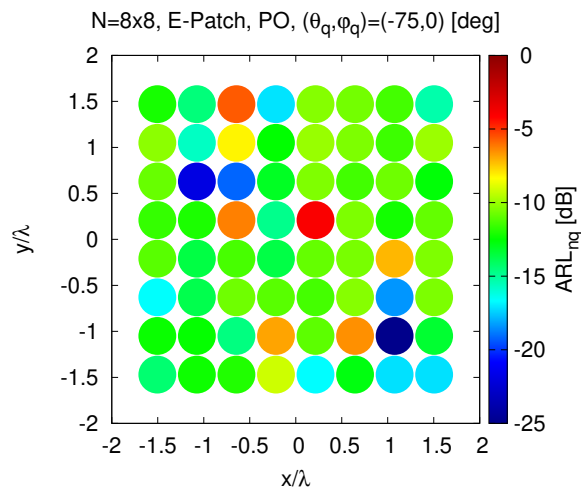
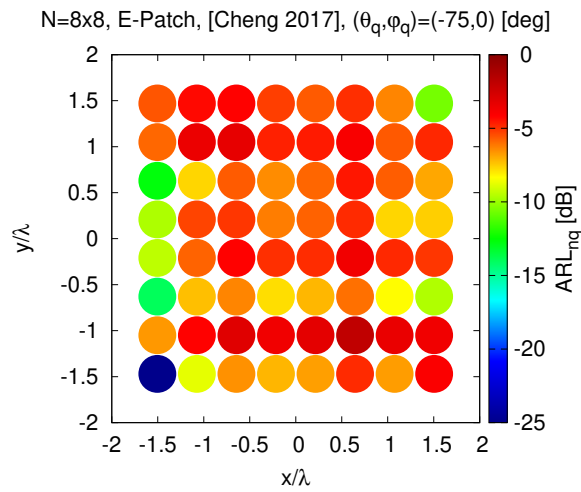


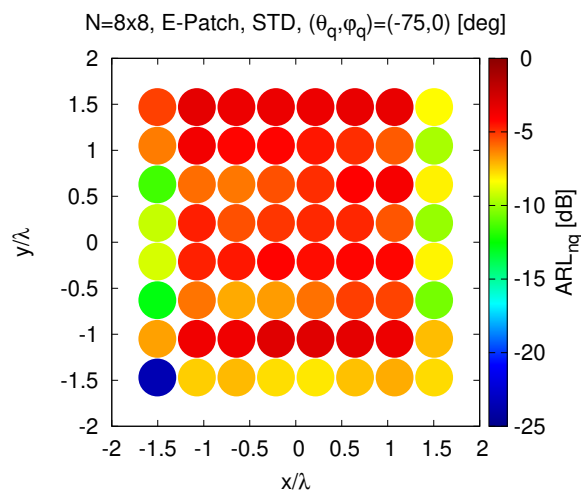
**Fig. 12** - P. Rosatti *et al.*, “Synthesis of Wide-Angle Scanning Arrays ...”



(a)



(b)



(c)

Fig. 13 - P. Rosatti *et al.*, “Synthesis of Wide-Angle Scanning Arrays ...”

$q$	$(\theta_q, \varphi_q)$	$\psi_q^{PO}(\theta_q, \varphi_q)$	$\psi_q^{[Cheng2017]}(\theta_q, \varphi_q)$	$\psi_q^{STD}(\theta_q, \varphi_q)$	$\zeta_q^{PO}$	$\zeta_q^{[Cheng2017]}$	$\zeta_q^{STD}$
4	(-75, 0)	41.83	35.97	41.40	2.98	27.62	28.30
8	(-55, 0)	41.32	22.79	41.45	13.42	23.35	24.30
30	(55, 0)	46.91	44.42	47.02	14.80	23.35	23.16
34	(75, 0)	46.76	40.83	46.91	17.28	27.43	26.68

**Tab. I - P. Rosatti *et al.*, “Synthesis of Wide-Angle Scanning Arrays ...”**

$q$	$(\theta_q, \varphi_q)$	$SLL_q^{PO}$	$SLL_q^{[Cheng\ 2017]}$	$SLL_q^{STD}$	$G_q^{PO}$	$G_q^{[Cheng\ 2017]}$	$G_q^{STD}$	$\Delta\Theta_q^{PO}$	$\Delta\Theta_q^{[Cheng\ 2017]}$	$\Delta\Theta_q^{STD}$
4	$(-75, 0)$	-2.12	-5.78	-5.38	6.57	6.56	7.38	3.55	4.03	3.75
8	$(-55, 0)$	-3.82	-5.68	-5.44	6.54	6.04	7.04	3.71	1.86	2.26
30	$(55, 0)$	-8.83	-10.06	-9.85	12.16	11.78	12.47	2.77	2.17	2.22
34	$(75, 0)$	-9.06	-9.29	-9.61	12.22	11.79	12.62	5.06	0.94	4.94

Tab. II - P. Rosatti *et al.*, "Synthesis of Wide-Angle Scanning Arrays ..."